arXiv:1503.08605v2 [cond-mat.quant-gas] 5 Nov 2015

Non-equilibrium dynamics of spin-orbit coupled lattice bosons

H. T. Ng
Center for Quantum Information, Institute for Interdisciplinary Information Sciences,
Tsinghua University, Beijing 100084, P. R. China

(Dated: November 6, 2015)

We study the non-equilibrium dynamics of two component bosonic atoms in a one-dimensional optical lattice in the presence of spin-orbit coupling. In the Mott insulating regime, the two-component bosonic system at unity filling can be described by the quantum spin XXZ model. The atoms are initially prepared in their lower spin states. The system becomes out of equilibrium by suddenly introducing spin-orbit coupling to the atoms. The system shows the relaxation and non-stationary dynamics, respectively, in the different interaction regimes. We find that the time average of magnetization is useful to characterize the many-body dynamics. The effects of even and odd numbers of sites are discussed. Our result sheds light on non-equilibrium dynamics due to the interplay between spin-orbit coupling and atomic interactions.

PACS numbers: 03.75.Lm, 03.75.Mn, 05.70.Ln

I. INTRODUCTION

Non-equilibrium dynamics of a closed many-body system is of fundamental importance [1, 2] in quantum physics and statistical mechanics. For example, the local observables appear to be in thermal states even if the entire many-body system is in a pure state. The eigenstate thermalization hypothesis [3–5] was proposed to explain such phenomena for complex quantum systems. However, it cannot be applied to integrable systems. In fact, a general mechanism of thermalization is still lacking [2]. It is important to study the dynamics of an isolated many-body system in experiments. This may help to understand the behaviour of non-equilibrium dynamics and thermalization mechanism.

Ultracold atoms offer experimental platforms to study many-body dynamics of closed systems [6]. For instance, ultracold atoms can provide a relatively long accessible time to study the non-equilibrium dynamics, and the high level of controllability to adjust the interaction parameters for initiating the many-body dynamics. In addition, ultracold atoms have been exploited to simulate a lot of intriguing quantum phenomena such as quantum phase transition [7] from a Mott insulating regime to superfluid. The advanced detection techniques have been invented to enable one to individually address a single atom [8, 9]. Therefore, this can be used for probing the dynamics in the microscopic description [10]. Recently, the relaxation dynamics of closed ultracold atomic systems have been observed [11, 12].

In this paper, we consider a system of two-component bosonic atoms in a one-dimensional (1D) optical lattice. In the Mott insulating regime, the system, with unit filling, can be described by a quantum spin XXZ model [13]. We consider all atoms to be initially prepared in their lower spin states. To study the non-equilibrium dynamics, the spin-orbit (SO) coupling [14] is suddenly turned on. In fact, SO coupling, which produces the interaction between the particle's spin and momentum, naturally exists in solid-state materials. It gives rise to a number of intriguing effects such as topological insulators and superconductors, etc. [15, 16]. Spin-orbit coupling in atomic Bose-Einstein condensates [17] can be produced by inducing two-photon Raman transition using a pair of lasers [18]. Alternatively, the SO coupling between the atoms in the lattice can be induced by periodically shaking the lattice potential [19, 20]. More recently, the techniques for adjusting SO coupling have been shown [21, 22]. The SO coupling gives rise to pair interactions between two neighbouring atoms and Dzyaloshinskii-Moriya (DM) interactions [23–27] in the lattice. The DM interaction leads to rich magnetic phase diagram [23], for example, it can induce spin spirals.

We consider the magnetization as an observable to study the many-body dynamics. We find that the time average of magnetization is useful for characterizing the non-equilibrium dynamics. The system exhibits the relaxation and non-stationary dynamics in the different interaction regimes which depend on the SO coupling strength and the ratio of inter-component interaction to intra-component interaction. Indeed, the dynamical behaviours relate to the overlap between the initial state and eigenstates. The interplay between the SO coupling and atomic interactions leads to the changes of this overlap, and results in the different dynamical behaviours.

Thermalization [28–31] occurs when a subsystem evolves to a mixed state even if the system is in a pure state. In the relaxation regime, the spins rapidly relax just after the SO coupling is turned on. The degree of quantum coherence of local spins can be measured by using the purity. An atom in each site will evolve to a nearly completely mixed state in a sufficiently long time.

The transition from the relaxation dynamics to non-stationary evolution occurs when the SO coupling strength is strong and the inter-component interaction strength becomes sufficiently larger than the intra-component interaction. In the non-stationary regime, we find that the distinct dynamics are displayed for the even and odd numbers of sites, respectively. For even-number cases, the effective two-level dynamics is shown. This forms a superposition of two distinct states [33] during the time evolution. These superposition states are useful for quantum metrology [34]. On the other hand, the spin system becomes ferromagnetic in the odd-number cases.

This paper is organized as follows: In Sec. II, we introduce the system. In Sec. III, we study the non-equilibrium dynamics of this system. We characterize the many-body dynamics by using the time average of magnetization. We discuss the relaxation dynamics of local spins and non-stationary dynamics in the different interaction regimes. The effects of even and odd number of sites on the dynamics are discussed. We provide a discussion and a conclusion in the sections IV and V, respectively. In Appendix A, we derive the effective Rabi frequency.

II. SYSTEM

We consider the two-component bosonic atoms to be trapped in a one-dimensional optical lattice. We assume that this system has open boundary conditions. The two-component Bose-Hubbard model can be used to describe the interactions of two-component bosons in an optical lattice. The Hamiltonian $H_{\rm BH}$ can be written as, ($\hbar = 1$),

$$H_{\rm BH} = \sum_{\alpha,i} \Big[J_\alpha(\alpha_i^\dagger \alpha_{i+1} + {\rm H.c.}) + \frac{U_\alpha}{2} n_i^\alpha (n_i^\alpha - 1) + U_{ab} n_i^a n_i^b \Big], \tag{1}$$

where α_i and $\alpha_i^\dagger$ are the annihilation and creation operators of an atom in the atomic spin state $|\alpha\rangle$, and n_i^α is the number operator at site i, and $\alpha = a, b$. The parameter J_α is the tunnel coupling, $U_{a(b)}$ and U_{ab} are the intra- and inter-component interaction strengths of atoms, respectively. We assume that the tunnel coupling and atom-atom interaction strength of each component are nearly equal, i.e., $J_a \approx J_b \approx J$ and $U_a \approx U_b \approx U$.

We consider that the atom-atom interaction strengths U and U_{ab} are repulsive, and also they are much larger than the parameters such as J and t_{so}. In this strongly interacting regime with unit filling, it is convenient to write the two-mode bosonic operators in terms of angular momentum operators, i.e., $S_i^+ = a_i^\dagger b_i$, $S_i^- = b_i^\dagger a_i$ and $S_i^z = (b_i^\dagger b_i - a_i^\dagger a_i)/2$. The Hamiltonian can be written in terms of spin operators as:

$$H_{\rm XXZ} = \lambda \sum_{i=1}^{N-1} \Big[2(1 - 2U_r) S_i^z S_{i+1}^z - (S_i^+ S_{i+1}^- + S_i^- S_{i+1}^+) \Big], \tag{2}$$

where $\lambda = 2J^2/U_{ab}$ and $U_r = U_{ab}/U$. The system can be described by the quantum XXZ model [32].

To study the non-equilibrium dynamics, we consider the SO coupling to be suddenly applied to the atoms. For a non-interacting single-particle Hamiltonian, it is given by

$$H^s_{\rm SO} = \frac{\mathbf{k}^2}{2m} I + \beta k_x \sigma_y + \delta k_y \sigma_x, \tag{3}$$

where $\mathbf{k} = (k_x, k_y, k_z)$ is the momentum of a particle with a mass m, β and δ are the SO coupling strengths, and I and $\sigma_{x,y}$ are the identity and the Pauli spin operators, respectively. If δ equals $-\beta$, then it is called as the Rashba SO coupling [17]. The Dresselhaus SO coupling [17] is an alternative form of spin-orbit coupling where β equals δ and they are both negative [17]. Recently, the SO coupling with an equal weight of Rashba and Dresselhaus couplings has been realized in a ^{87}Rb Bose-Einstein condensate [17], i.e., $\beta \neq 0$ and $\delta = 0$. By inducing a two-photon Raman transition via the laser beams, the equal weight of Rashba and Dresselhaus SO couplings can be produced, $\propto k_x \sigma_y$. The Hamiltonian, which describes such SO coupling in a 1D optical lattice, can be written as [35, 36]

$$H_{\rm SO} = t_{so} \sum_i (a_i^\dagger b_{i+1} - a_i^\dagger b_{i-1} + {\rm H.c.}), \tag{4}$$

where t_{so} is the strength of spin-orbit coupling.

In the presence of SO coupling, the effective Hamiltonian is written as [25, 26]

$$\begin{aligned} H^s_{\rm eff} = \lambda \sum_{i=1}^{N-1} \Big\{ & 2\Big[\Big(\frac{t_{so}}{J}\Big)^2 - 1\Big]\Big(2U_r - 1\Big) S_i^z S_{i+1}^z \\ & + \Big(\frac{t_{so}}{J}\Big)^2 (S_i^+ S_{i+1}^+ + S_i^- S_{i+1}^-) - (S_i^+ S_{i+1}^- + S_i^- S_{i+1}^+) \\ & - 4\frac{U_{ab}}{U}\Big(\frac{t_{so}}{J}\Big)(S_i^z S_{i+1}^x - S_i^x S_{i+1}^z) \Big\}. \end{aligned} \tag{5}$$

The last terms in Eq. (5) are called the DM interactions [25, 26]. Now the total system can be described by the XYZ spin model with the DM interactions [25–27].

Let us briefly discuss the various terms in the effective Hamiltonian in Eq. (5). The first term $S_i^z S_{i+1}^z$ favors to preserve the same polarization of two neighboring spins with their initial states. This gives rise to bound magnons in the XXZ chain [10]. The second term $S_i^+ S_{i+1}^+ + S_i^- S_{i+1}^-$ describes the interaction which excites and de-excites the two neighboring spins in pair simultaneously. The third term $S_i^+ S_{i+1}^- + S_i^- S_{i+1}^+$ leads to spin-exchange between two nearest neighbors. The forth term $S_i^z S_{i+1}^x - S_i^x S_{i+1}^z$ causes spin-rotation in which the rotation direction depends on the spin states of their nearest neighbors.

When t_{so}/J and U_r are roughly equal to one, all terms equally contribute to the dynamics. All the terms are in competition. This results in eigenstates with the different combinations of spin states. On the contrary, when both parameters t_{so}/J and U_r are large, the first term becomes dominant. All spins tend to have the same polarization. This leads to the very different dynamics in these two interaction regimes.

III. MANY-BODY DYNAMICS

We investigate the quantum dynamics of the system by suddenly applying the SO coupling to the atoms. Initially, all atoms are prepared in their lower spin states, i.e.,

$$|\Psi(0)\rangle = |\downarrow\downarrow\ldots\downarrow\downarrow\rangle. \tag{6}$$

This state is indeed an eigenstate in Eq. (2) for $t_{so}=0$. To initiate non-equilibrium dynamics, a quantum quench has to be introduced. By suddenly turning on the SO coupling, the system is described by the Hamiltonian in Eq. (5). The initial state is no longer an eigenstate of the Hamiltonian of the system. If the SO coupling is suddenly turned on, then the system becomes out of equilibrium. We numerically simulate the dynamics of this spin chain by using exact diagonalization (see [37] and references therein).

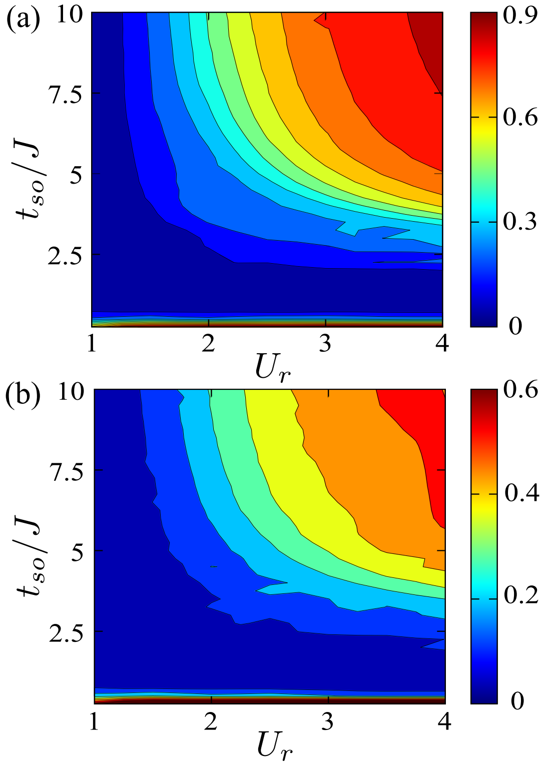

FIG. 1. (Color online) Contour plot of the average of magnetization $|M|$ versus parameters t_{so} and U_r, where the total time taking for average is $\tau = 10\lambda$. The system's sizes $N = 11$ and $N = 12$ are shown in (a) and (b), respectively.

We study the dynamics of magnetization which is given by

$$M = \frac{2}{N}\sum_{i=1}^{N}\langle S_i^z\rangle. \tag{7}$$

The magnetization M is equal to $+1(-1)$ when all spins are in up(down) states. We take the average of magnetization $|M|$ within a period $\tau = 10\lambda$, i.e.,

$$\bar{M} = \frac{1}{\tau}\int_0^{\tau}|M(t)|dt. \tag{8}$$

By taking the absolute sign of the magnetization, we can ensure that $\bar{M}$ is positive. Here we set the period τ to be 10λ. This period is sufficiently long until the local spins become steady. It enables us to characterize the dynamics by using $\bar{M}$ in Eq. (8).

In Fig. 1, we plot the time average of magnetization $\bar{M}$ versus the parameters t_{so} and U_r. When t_{so}/J ranges from 0.75 to 2, $\bar{M}$ is close to zero. Note that the initial magnetization is -1. After taking the average, it becomes nearly zero. This means that the system reaches a steady state and the magnitude of magnetization is small in a long time.

As both t_{so} and U_r increase, $\bar{M}$ gradually increases. The system is no longer stationary in a long time. This shows the different layers in Fig. 1. When both parameters t_{so}/J and U_r become sufficiently large, $\bar{M}$ can reach nearly 0.5 and 1, respectively, for the even and odd numbers of sites. In this regime, this shows that the different behaviours of even- and odd-number of sites.

It should be noted that the average magnetization is close to one in Fig. 1 if t_{so}/J is less than 0.75. In fact, we cannot characterize the dynamics of this interaction range because the time evolution is too slow and they do not reach the steady state within the period $\tau = 10\lambda$.

According to Fig. 1, the many-body dynamics can be mainly classified into the two different types which are relaxation dynamics and non-stationary evolution, respectively. We will discuss them in the following subsections.

A. Relaxation dynamics

Now we study the quantum dynamics of local spins in the parameter region which the long-time average of magnetization $\bar{M}$ is about zero in Fig. 1. In Figs. 2(a) and (b), we plot the dynamics of magnetization M, for the odd and even numbers of sites, respectively. Initially, the magnetization M is equal to -1. When the SO coupling is turned on, the magnetization swiftly increases in a short time. Then, it becomes saturated to around zero in a longer time. This shows that the spins nearly relax to the steady states. As the system size increases, the magnetization becomes more steady. Besides, the relaxation dynamics shows no different in the odd- and even-number cases.

To study the relaxation of local spins, we examine their purities. The purity is a quantity which measures the degree of quantum coherence of a system. It is defined as

$$\Lambda_{\rm pur} = {\rm Tr}(\rho^2), \tag{9}$$

where ρ is the density matrix of a system. If the system is in a pure state, then the purity is equal to one. Otherwise, the purity is less than one.

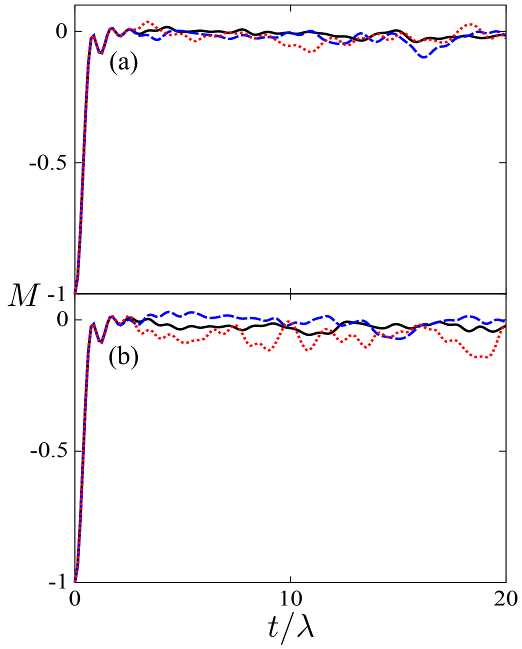

FIG. 2. (Color online) Magnetization M versus time t/λ, for $t_{so} = J$ and $U_r = 1$. The odd and even numbers of sites are shown in (a) and (b). The different sizes of the system are denoted with the different lines: $N = 11$ and 12 (red dotted), $N = 13$ and 14 (blue dashed) and $N = 15$ and 16 (black solid), respectively.

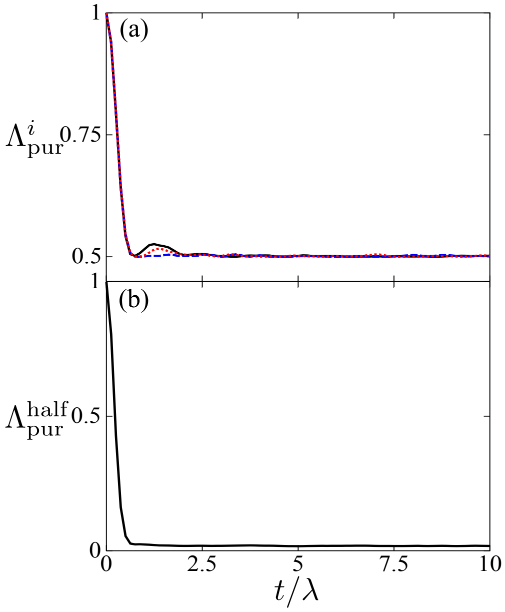

FIG. 3. (Color online) Purities of local spins and half of a spin chain versus time t/λ. In (a), the purity of local spin i versus dimensionless time t/λ is shown. The different lines are denoted for the purities of different ion i: $i = 4$ (solid black), $i = 6$ (blue dashed) and $i = 8$ (red dotted), respectively. In (b), the purity of the left part of a spin chain versus time is plotted. The parameters are used: $N = 12$, $t_{so} = J$ and $U_r = 1$.

We investigate the purity $\Lambda^i_{\rm pur}$ of ion i, where $\Lambda^i_{\rm pur} = {\rm Tr}(\rho_i^2)$ and ρ_i is the reduced density matrix of ion i. The reduced density matrix ρ_i can be obtained by tracing out the rest of the other spins in the chain. In Fig. 3(a), we plot the purities of local spins versus time. The initial purity is equal to 1. Afterwards, the purities rapidly drop and the purity $\Lambda^i_{\rm pur}$ of a local spin decreases to about 0.5 in a long time. The purity of a spin-half particle in a completely mixed state is 0.5, where all diagonal elements of ρ_i are equally weighted and off-diagonal elements are zero. This implies that the spins are nearly fully relaxed. Additionally, we study the purity $\Lambda^{\rm half}_{\rm pur} = {\rm Tr}(\rho^2_{\rm half})$ of a half of the spin chain in Fig. 3(b), where the reduced density matrix $\rho_{\rm half}$ can be obtained by tracing out another half of the chain. The purity becomes saturated to a value 0.018. It is very close to the totally mixed state which gives the purity $\Lambda^{\rm half}_{\rm pur} = 2^{N/2-N} \approx 0.015625$ in our case. This means that the half of a spin chain can be approximately described by a totally mixed state.

Then, we compare the relaxation dynamics with the different strengths of parameters U_r. The average magnetization $\bar{M}$ increases when U_r becomes larger. In Fig. 4(a), we plot the magnetization M as a function of time, for $U_r = 1$ and 1.5, respectively. The magnetization M in Eq. (7) fluctuates around zero with a larger magnitude if U_r becomes larger. Therefore, this will give a larger value of $\bar{M}$ in Eq. (8) which is obtained by taking average of the absolute value of M. We study the purity of a local spin in Fig. 4(b). The purity increases when U_r increases. This means that this local spin has a higher degree of quantum coherence. This suggests that $\bar{M}$ is an useful quantity to characterize the relaxation dynamics of this system.

Indeed, the occurrence of relaxation can be understood by examining the overlap between the initial state and eigenvectors of the system. We consider the probability coefficients of the initial state and eigenvectors

$$P_n = |\langle\Psi(0)|E_n\rangle|^2, \tag{10}$$

where $|\Psi(0)\rangle$ and $|E_n\rangle$ are the initial state and the n-th eigenvectors.

In Fig. 5(a), we plot the overlap probabilities P_n versus n, where $t_{so}/J = U_r = 1$ and n is an index of the n-th eigenstate. This corresponds to the previous case in Fig. 2. We can see that the initial state has a large overlap with the eigenstates. The initial state overlaps with almost entire eigen-spectrum. In Fig. 5(b), the overlap probabilities P_n are plotted versus n. It corresponds to the case in Fig. 4, where the magnetization shows stronger fluctuations in the dynamics. Obviously, the overlap between the initial state and the eigenstates is much smaller than that in Fig 5(a). Here the off-diagonal terms of the observables are suppressed if there is a large overlap between the initial states and the eigenstates of the system.

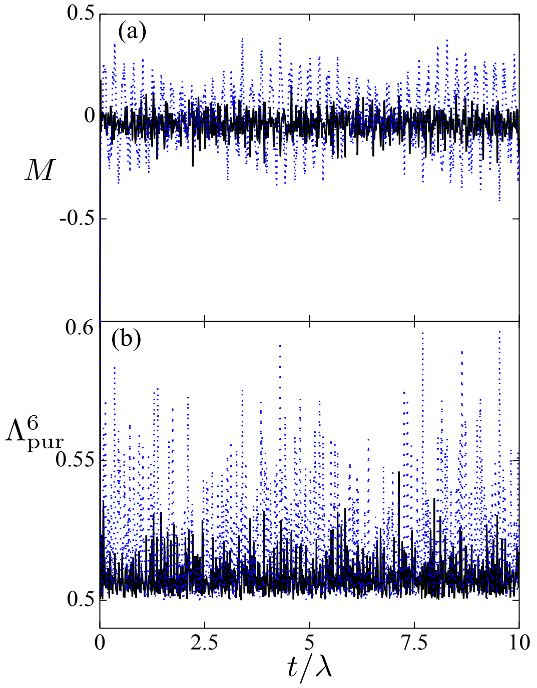

FIG. 4. (Color online) Magnetization M and purity $\Lambda^6_{\rm pur}$ of the 6-th spin versus time t/λ are plotted in (a) and (b), respectively, for $N = 12$ and $t_{so} = 8J$. The different parameters $U_r = 1$ and $U_r = 1.5$ are denoted with the black-solid and blue-dotted lines, respectively.

B. Even-odd effect

When both parameters t_{so}/J and U_r are sufficiently large, the dynamics of the system becomes non-stationary. We find that the dynamical behaviours are totally different between the even and odd numbers of sites. For even-number cases, the system undergoes an effective two-level dynamics. In contrast, the system becomes ferromagnetic if the number of sites is odd.

1. *Even number case: Effective two-level dynamics*

When t_{so}/J and U_r are both larger than one, the first term in the Hamiltonian in Eq. (5) becomes dominant, i.e., $H_0 \propto \sum_i S^z_i S^z_{i+1}$ and the other terms in the Hamiltonian are perturbations. Obviously, the states $(|\uparrow\uparrow\ldots\uparrow\uparrow\rangle \pm |\downarrow\downarrow\ldots\downarrow\downarrow\rangle)/\sqrt{2}$ are two nearly degenerate eigenstates of the Hamiltonian H_0. In this regime, the entire many-body dynamics can be effectively described by these two degenerate states if the system starts with $|\downarrow\downarrow\ldots\downarrow\downarrow\rangle$ in Eq. (6). We plot the time evolution of the magnetization in Fig. 6(a). The magnetization shows periodic oscillations. The effective Rabi frequency decreases as the parameter U_r increases and a larger magnitude can be attained. In fact, the superposition of the two degenerate ground states can be produced, i.e.,

$$|\Psi(t)\rangle \approx c_1|\uparrow\uparrow\ldots\uparrow\uparrow\rangle + c_2|\downarrow\downarrow\ldots\downarrow\downarrow\rangle, \qquad (11)$$

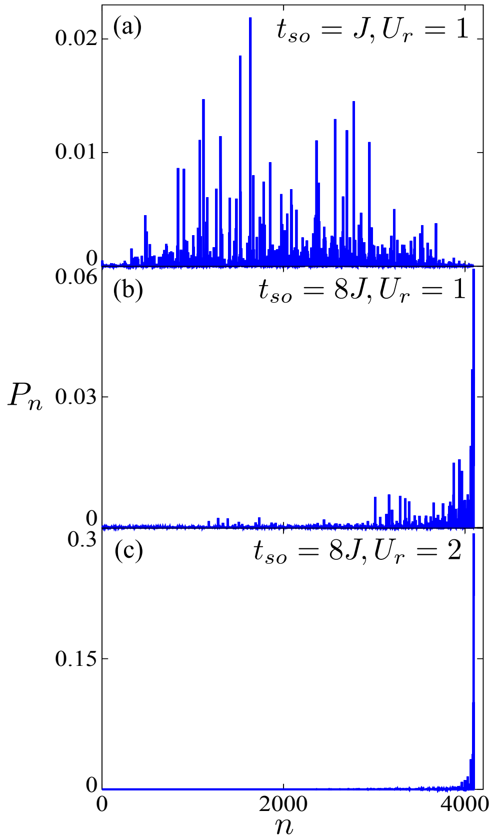

FIG. 5. (Color online) Overlap probability P_n versus the index n of the n-th eigenstate, for $N = 12$. In (a), the parameters $t_{so} = J$ and $U_r = 1$ are used. The different parameters $U_r = 1$ and 2 are used in (b) and (c), respectively, but with the same SO coupling, $t_{so} = 8J$.

where $|c_1|^2 + |c_2|^2 = 1$.

The two degenerate states can be coupled via the high-order virtual transitions. The effective Rabi frequency can be approximately obtained which can be derived by using the high-order perturbation theory in Appendix A. Since this effective Rabi frequency inversely scales with the power N, the rate of evolution becomes slow as the system's size increases. This hinders the creation of superposition of two spin states when the system goes large.

In Fig. 5(c), we plot the overlap between the initial state in Eq. (6) and the eigenstates. The overlap is much smaller than the two previous cases in Figs. 5(a) and (b) which shows the relaxation dynamics. We have presumed that the system is strictly contained in the degenerate subspace which can be described by the two degenerate states only. Therefore, there are only two degenerate states involved in the entire dynamics. In the limit of strong interaction, the dynamics cannot be thermalized.

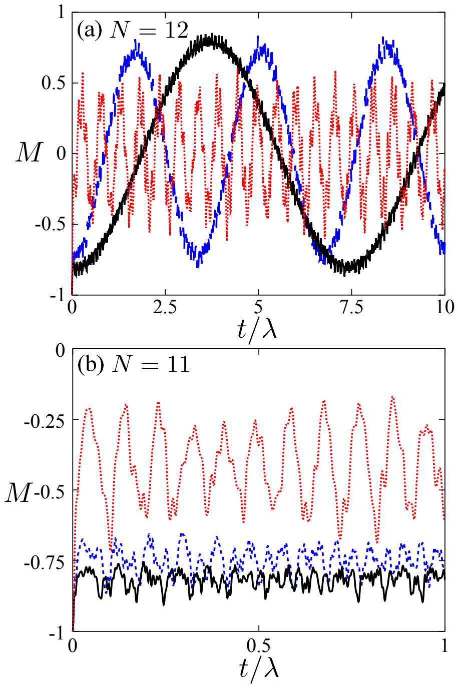

FIG. 6. (Color online) Magnetization $\tilde{M}$ versus time t/λ for even ($N = 12$) and odd ($N = 11$) numbers in (a) and (b), respectively, and $t_{so} = 8J$. The different lines for the different U_r are shown: $U_r = 4$ (black solid line), $U_r = 3$ (blue dash line) and $U_r = 2$ (red dotted line), respectively.

2. *Odd number case: Ferromagnetic*

In Fig. 6(b), we plot the magnetization versus time for odd-number cases. The spins tend to maintain in their ground states when U_r increases. The spin system is ferromagnetic. Indeed, the initial state in Eq. (6) is an eigenstate if the parameters t_{so} and U_r go large. Therefore, the magnetization is about -1 for the large values of t_{so} and U_r. The small fluctuations around -1 are shown due to the virtual transitions from the perturbed terms.

The odd- and even-number cases are totally different to each other. In even-number cases, the effective two-level dynamics occurs due to the virtual fluctuations of the perturbation terms $\sum_i S_i^+ S_{i+1}^+$+H.c.. However, these perturbation terms alter the spin state in pair only and therefore they cannot contribute the dynamics between the two degenerate states $|\uparrow\uparrow \ldots \uparrow\rangle$ and $|\downarrow\downarrow \ldots \downarrow\rangle$ for odd-number cases. Also, the DM terms cancel the contributions from the spin states and their reflection states. For example, the states $|001\rangle$ and its reflection states $|100\rangle$ will be cancelled in the perturbation series. Therefore, the DM terms cannot lead to the effective two-level dynamics in this case.

IV. DISCUSSION

We have investigated the non-equilibrium dynamics of a closed quantum system by suddenly applying the SO coupling. It is necessary to produce and tune the required SO couplings to the atoms. There are several ways to create SO coupling such as two-photon Raman transition [17, 18] and shaking lattice [19, 20]. Recently, the techniques for tuning SO coupling [21] have been demonstrated by using Raman coupling with laser fields. However, this method may produce unwanted heating due to spontaneous emissions of atoms.

Alternatively, the SO coupling can be exploited by shaking the lattice periodically. This “shaking” method has been used to successfully generate the artificial gauge potential to cold atoms in lattices [38]. More recently, the theoretical proposals for the realization of SO coupling have been put forward [19, 20]. This method is able to create SO coupling without heating if the appropriate driving conditions are met [19]. The other scheme, which overcomes the problems of spontaneous emissions, has also been proposed [39]. Apart from that, it is also required to adjust the inter- and intra-component interaction strengths for observing the different kinds of dynamics. This can be made by using Feshbach resonance [40]. The scattering length between the different components of atoms can be modified by applying the appropriate magnetic fields to the atoms [41].

In addition, we make a rough estimation of the relaxation time-scale in realistic experiments. We take the typical value of the tunnel coupling J to be about 100∼200 Hz in optical-lattice experiments[10, 42]. Since the ratio U_{ab}/J is tunable [7], we assume that it ranges between 5 to 10 to enter the Mott insulator regime. This gives the parameter $\lambda = 2J^2/U_{ab}$ to be roughly about 40 to 80 Hz. In Fig. 2, we can see that the system takes the period λ for relaxation which is about $10 \sim 20$ ms. To observe the intrinsic effect of relaxation in an isolated system, the relaxation time must be much shorter than the damping time from the external noise sources. The typical heating time of atoms in optical lattice is several hundreds of ms [10]. This suggests that the relaxation of local spins can be detected in experiments. To take the time-average of magnetization, the required time is about $10\lambda \sim 100$ ms which is comparable to the heating time. In realistic experiments, the average time of extracting the magnetization can be chosen to be shorter than the heating time to characterize the dynamical properties of the system.

V. CONCLUSION

In summary, we have studied the many-body dynamics of two-component bosonic atoms in a 1D optical lattice by suddenly introducing the SO coupling. In Mott-insulating regime, the system can be described by a quantum spin system. We study the dynamics of magnetization of the system. We find that the time average of magnetization is useful for characterizing the non-equilibrium dynamics. The system shows the relaxation and non-stationary dynamics in the different interaction regimes. In the relaxation regime, the magnetization becomes nearly stationary in a long time and the local spins become nearly fully relaxed. When the SO coupling is strong and the inter-component interaction strength is sufficiently larger than the intra-component strength, the system becomes non-stationary. The totally different dynamical behaviours are shown for the even and odd numbers of sites in the non-stationary regime.

Appendix A: Derivation of effective Rabi frequency

We study the effective Rabi frequency between the two degenerate states from the perturbation theory. We consider the pair-excitation interaction V to be perturbation. The Hamiltonian $H^s_{\rm eff} \approx H_0 + V$, where H_0 and V are given by

$$\begin{aligned} H_0 &= \lambda \sum_{i=1}^{N-1} \Big\{ 2\Big[\Big(\frac{t_{so}}{J}\Big)^2 - 1\Big]\Big(2\frac{U_{ab}}{U} - 1\Big) S^z_i S^z_{i+1}, \\ V &= \lambda \Big(\frac{t_{so}}{J}\Big)^2 (S^+_i S^+_{i+1} + S^-_i S^-_{i+1}), \end{aligned} \tag{A1}$$

where H_0 is treated as an unperturbed Hamiltonian and V as a perturbation.

To calculate the effective Rabi frequency, we need to evaluate the virtual transition from $|\uparrow\uparrow \dots \uparrow\rangle$ and $|\downarrow\downarrow \dots \downarrow\rangle$. The perturbation term V can make the transitions for two neighboring spins in pair. It takes $N/2$ virtual transitions from $|\uparrow\uparrow \dots \uparrow\rangle$ and $|\downarrow\downarrow \dots \downarrow\rangle$ only. We can then make the approximation by using the $N/2$-th order perturbation theory. However, the DM terms will take N virtual transitions to connect these two states. The N-th order perturbation theory has to be used. The correction from the DM terms is much smaller than that from the term V. Therefore, we can safely ignore the DM terms in calculating the perturbation theory if t_{so}/J is comparable with U_{ab}/U.

We can obtain the leading terms of the $N/2$-th order eigenenergy:

$$\begin{aligned} E^{(N/2)}_{n_1,n_2} = &\sum_{j=1}^{\tilde{N}_c} \frac{V_{n_2 k_{N/2-1}} (\prod_{i=1}^{N/2-1} V^j_{k_{i+1}k_i}) V^j_{k_1 n_1}}{\prod_{i=1}^{N/2-1} E^j_{l_D k_i}} \\ &+\text{other terms}, \end{aligned} \tag{A2}$$

where $V^j_{lk} = {}_j\langle l|V|k\rangle_j$, $E^j_{lk} = E^{(0)}_{l_D} - E^{(0)}_{k_j}$ and D denotes the degenerate subspace for $n_1 = |\uparrow\uparrow \dots \uparrow\rangle$ and $n_2 = |\downarrow\downarrow \dots \downarrow\rangle$, and $\tilde{N}_c$ is the number of possible terms that connect the two degenerate states via virtual fluctuations. The number $\tilde{N}_c$ can be obtained numerically by counting all possibilities to connect the two states. The leading term of $E^{(N/2)}_{n_1,n_2}$ can be written as

$$E^{(N/2)}_{n_1,n_2} \approx \lambda \Big(\frac{t_{so}}{J}\Big) 2^{1-N/2} (2U_r - 1)^{1-N/2} \tilde{N}_c. \tag{A3}$$

TABLE I. This table shows the effective Rabi frequencies from the numerical results and the perturbation theory for the different system's sizes, and the percent error η.

N	Ω_R/λ	$\tilde{\Omega}_R/\lambda$	η
6	8.9760	8.1633	9.1%
8	2.7013	2.3324	13.7%
10	0.83642	0.66639	20.3%
12	0.25964	0.19040	26.7%

We compare the effective Rabi frequency between the numerics and the approximation from the perturbation theory in Table I, for the different sizes N. The percent error η shows the error between the exact numerical value and the approximation. It is defined as

$$\eta = \frac{|\Omega_R - \tilde{\Omega}_R|}{|\Omega_R|} \times 100\%. \tag{A4}$$

Here we denote $\tilde{\Omega}_R = E^{(N/2)}_{n_1,n_2}$ as the approximation from the perturbation theory. This approximation is fairly good when N is small. However, as N increases, the error grows. In fact, we have taken account of the leading term from the $N/2$-th order perturbation only. When N increases, the calculation should include the higher order perturbation terms to improve the accuracy.

ACKNOWLEDGMENTS

This work was supported in part by the National Basic Research Program of China Grant No. 2011CBA00300 and No. 2011CBA00301, and the National Natural Science Foundation of China Grant No.11304178, No. 61061130540, and No. 61361136003.

[1] A. Polkovnikov, K. Sengupta, A. Silva and M. Vengalattore, Rev. Mod. Phys. **83**, 863 (2011).
[2] J. Eisert, M. Friesdorf and C. Gogolin, Nat. Phys. **11**, 124 (2015).
[3] J. M. Deutsch, Phys. Rev. A **43**, 2046 (1991).
[4] M. Srednicki, Phys. Rev. E **50**, 888 (1994).
[5] M. Rigol, V. Dunjko and M. Olshanii, Nature **452**, 854 (2008).
[6] T. Langen, R. Geiger, J. Schmiedmayer, arXiv:1408.6377.
[7] M. Greiner, O. Mandel, T. Esslinger, T. W. Hänsch and I. Bloch, Nature **415**, 39 (2002).

[8] W. S. Bakr, J. I. Gillen, A. Peng, S. Fölling and M. Greiner, Nature **462**, 74 (2009).

[9] C. Weitenberg, M. Endres, J. F. Sherson, M. Cheneau, P. Schauß, T. Fukuhara, I. Bloch and S. Kuhr, Nature **471**, 319 (2011).

[10] T. Fukuhara, P. Schauß, M. Endres, S. Hild, M. Cheneau, I. Bloch and C. Gross, Nature **502**, 76 (2013).

[11] S. Trotzky, Y-A. Chen, A. Flesch, I. P. McCulloch, U. Schollwck, J. Eisert and I. Bloch, Nat. Phys. **8**, 325 (2012).

[12] M. Gring, M. Kuhnert, T. Langen, T. Kitagawa, B. Rauer, M. Schreitl, I. Mazets, D. Adu Smith, E. Demler, J. Schmiedmayer, Science **337**, 1318 (2012).

[13] U. Schollwöck *et al.*, *Quantum magnetism* (Berlin, Springer, 2004).

[14] V. Galitski and I. B. Spielman, Nature **494**, 49 (2013).

[15] M. Z. Hasan and C. L. Kane, Rev. Mod. Phys. **82**, 3045 (2010).

[16] X.-L. Qi and S.-C. Zhang, Rev. Mod. Phys. **83**, 1057 (2011).

[17] Y.-J. Lin, K. Jiméenz-García and I. B. Spielman, Nature **471**, 83 (2011).

[18] X.-J. Liu, M. F. Borunda, X. Liu, and J. Sinova, Phys. Rev. Lett. **102**, 046402 (2009).

[19] J. Struck, J. Simonet, K. Sengstock, Phys. Rev. A **90**, 031601 (2014).

[20] N. Goldman and J. Dalibard, Phys. Rev. X **4**, 031027 (2014).

[21] K. Jiménez-García, L. J. LeBlanc, R. A. Williams, M. C. Beeler, C. Qu, M. Gong, C. Zhang, I. B. Spielman, Phys. Rev. Lett. **114**, 125301 (2015).

[22] X. Luo, L. Wu, J. Chen, Q. Guan, K. Gao, Z.-F. Xu, L. You, R. Wang, arXiv:1502.07091.

[23] W. S. Cole, S. Zhang, A. Paramekanti and N. Trivedi, Phys. Rev. Lett. **109**, 085302 (2012).

[24] J. Radić, A. D. Ciolo, K. Sun and V. Galitski, Phys. Rev. Lett. 109, 085303 (2012).

[25] M. Piraud, Z. Cai, I. P. McCulloch, and U. Schollwöck, Phys. Rev. A **89**, 063618 (2014).

[26] J. Z. Zhao, S. J. Hu, J. Chang, F.W. Zheng, P. Zhang, and X. Q. Wang, Phys. Rev. B **90**, 085117 (2014).

[27] H. T. Ng, Phys. Rev. A **90**, 053625 (2014).

[28] S. Goldstein, J. L. Lebowitz, R. Tumulka and N. Zangh, Phys. Rev. Lett. **96**, 050403 (2006).

[29] S. Popescu, A. J. Short and A. Winter, Nat. Phys. **2** 754 (2006).

[30] S. Genway, A. F. Ho, and D. K. K. Lee, Phys. Rev. Lett. **105**, 260402 (2010).

[31] M. C. Bañuls, J. I. Cirac, M. B. Hastings, Phys. Rev. Lett. **106**, 050405 (2011).

[32] L.-M. Duan, E. Demler and M. Lukin, Phys. Rev. Lett. **91**, 090402 (2003).

[33] A. J. Leggett, J. Phys.: Condens. Matter **14**, R415 (2002).

[34] V. Giovannetti, S. Lloyd and L. Maccone, Science **306**, 1330 (2004).

[35] Z. Cai, X. Zhou, and C. Wu, Phys. Rev. A **85**, 061605(R) (2012).

[36] X.-J. Liu, Z.-X. Liu and M. Cheng, Phys. Rev. Lett. **110**, 076401 (2013).

[37] J. Schachenmayer, B. P. Lanyon, C. F. Roos, A. J. Daley, Phys. Rev. X **3**, 031015 (2013).

[38] J. Struck, C. Ölschläger, M. Weinberg, P. Hauke, J. Simonet, A. Eckardt, M. Lewenstein, K. Sengstock, and P. Windpassinger, Phys. Rev. Lett. **108**, 225304 (2012)

[39] C. J. Kennedy, G. A. Siviloglou, H. Miyake, W. C. Burton and W. Ketterle, Phys. Rev. Lett. **111**, 225301 (2013).

[40] C. Chin, R. Grimm, P. Julienne, and E. Tiesinga, Rev. Mod. Phys. **82**, 1225 (2010).

[41] M. Erhard, H. Schmaljohann, J. Kronjäger, K. Bongs, and K. Sengstock, Phys. Rev. A **69**, 032705 (2004).

[42] P. M. Preiss *et al.*, Science **347**, 1229 (2015).